Thermal expansion, heat capacity and magnetostriction of RAl$_3$ (R = Tm, Yb, Lu) single crystals.

S L Bud'ko[1], J C Frederick[1], E D Mun[1], P C Canfield[1] and G M Schmiedeshoff[2]

[1]Ames Laboratory US DOE and Department of Physics and Astronomy, Iowa State University, Ames, IA 50011, USA

[2]Department of Physics, Occidental College, Los Angeles, CA 90041, USA

Abstract. We present thermal expansion and longitudinal magnetostriction data for cubic RAl$_3$ (R = Tm, Yb, Lu) single crystals. The thermal expansion coefficient for YbAl$_3$ is consistent with an intermediate valence of the Yb ion, whereas the data for TmAl$_3$ show crystal electric field contributions and have strong magnetic field dependencies. de Haas-van Alphen-like oscillations were observed in the magnetostriction data of YbAl$_3$ and LuAl$_3$, several new extreme orbits were measured and their effective masses were estimated. Zero and 140 kOe specific heat data taken on both LuAl$_3$ and TmAl$_3$ for $T \leq 200$ K allow for the determination of a CEF splitting scheme for TmAl$_3$.

1. Introduction

Rare earth trialuminides, RAl$_3$, have been studied for several decades. The crystal structure of these materials is very sensitive to the rare earth ionic radius and it changes from hexagonal for light rare earths to cubic (Cu$_3$Au - type) for TmAl$_3$, YbAl$_3$, LuAl$_3$ (and ScAl$_3$) [1], with ErAl$_3$ reported to have been synthesized in both crystallographic variants [1, 2, 3]. TmAl$_3$ was reported to have a singlet ground state [3, 4]: the magnetic susceptibility follows the Curie-Weiss law with the magnetic moment corresponding to that of Tm^{3+} at high temperatures and becomes a temperature-independent Van Vleck type at low temperatures. YbAl$_3$, an intermediate valence compound [5] with the high Kondo temperature, T_K, of 600-700 K, recently experienced a revival of interest to its physical properties [6, 7, 8, 9] based, in part, on the uncovering of a second, low temperature, energy scale, Fermi liquid coherence ($T_{coh} \approx 40$ K), and slow crossover between T_K and T_{coh} [10].

Whereas many physical properties were measured and analyzed for cubic trialuminides, thermal expansion and magnetostriction data for these materials, in particular at low temperatures, appear to be absent from the literature (except for an early report [11] on the thermal expansion of LuAl$_3$ and YbAl$_3$ between $\sim$ 90 K and $\sim$ 800 K). In addition, for TmAl$_3$ the exact crystal electric field (CEF) splitting of the Hund's rule, ground state multiplet has remained unresolved [4, 12, 13, 14], in part due to a lack of high temperature and high magnetic field specific heat data. In this work we report extensive measurements of specific heat as well as thermal expansion and magnetostriction data for RAl$_3$ (R = Tm, Yb, Lu) single crystals so as to compare with other salient physical properties and to inquire into the effects of the CEF and intermediate valence (IV) on these characteristics. Simple crystal structure and the ability to synthesize large, high quality, singly crystals facilitate this endeavor.

2. Experimental methods

Large ($>$ 0.1 cm^3) single crystals (Fig. 1, inset) of RAl$_3$ (R = Tm, Yb, Lu) and R'$_{0.1}$Lu$_{0.9}$Al$_3$ (R' = Er, Tm, Yb) were grown from aluminum-rich binary (R - Al) or ternary (R' - Lu - Al) melts using a self-flux method [15]. High purity R (Ames Lab) and Al were placed, in atomic ratios of R$_{0.12}$Al$_{0.88}$ or (Lu$_{0.9}$R$_{0.1}$)$_{0.12}$Al$_{0.88}$, in alumina crucibles. These were sealed in fused quartz ampoules under a 1/3 atmosphere partial pressure of Ar. The ampoules were heated to 1050°C and then cooled to 675°C over 150 - 160 hours, at which point they were removed from the furnace and the excess Al was decanted. For R'$_{0.1}$Lu$_{0.9}$Al$_3$ with R' = Er, Tm the nominal concentration of R' was corroborated by the Curie-Weiss fit of the high temperature susceptibility. The inset to Fig. 1 shows crystals with clear, cubic morphology and mirrored (100) facets. Linear dimensions as large as 7 mm were commonly achieved.

Thermal expansion and magnetostriction were measured using a capacitive

dilatometer constructed of OFHC copper; a detailed description of the dilatometer is presented elsewhere [16]. The dilatometer was mounted in a Quantum Design PPMS-14 instrument and was operated over a temperature range of 1.8 to 300 K in an applied magnetic field up to 140 kOe. The samples were mounted in such a way that thermal expansion was measured along the [100] direction. The applied magnetic field was also along [100] such that $H \| L \| [100]$. The crystals were cut and polished so that the typical distance between the parallel (100) surfaces of the samples was $L_{[100]} \approx 2 - 3$ mm. Heat capacity of the samples was measured using a hybrid adiabatic relaxation technique of the heat capacity option in a Quantum Design PPMS-14.

Thermodynamic properties of materials are frequently analyzed using the concept of a Grüneisen function (or a Grüneisen parameter) [17]. For a single salient energy scale, ε, the Grüneisen parameter, γ, is defined as $\gamma = -d \ln \varepsilon / d \ln V$, where V is a molar volume. Using thermodynamic relations, we can obtain $\gamma(T, V) = \beta V / \chi_S C_p$, where β is a volume thermal expansion coefficient ($\beta = (\partial ln\ V / \partial T)_P$), χ_S is an adiabatic compressibility ($\chi_S = -(\partial ln\ V / \partial P)_S$) and C_p is a heat capacity at a constant pressure. For cubic materials $\gamma(T, V) = 3\alpha V / \chi_S C_p$, where α is a linear thermal expansion coefficient ($\alpha = (\partial ln\ a / \partial T)_P$, a - is a lattice parameter). Sometimes, in the analysis of experimental data, lacking the temperature-dependent compressibility data, the temperature dependence of the Grüneisen parameter can be approximated [19] as being proportional to β / C_p (or $3\alpha / C_p$ for cubic materials) under the assumption that the relative temperature dependence of χ_S is significantly smaller then that of thermal expansion coefficient or heat capacity. We will adopt such approach in this work.

If more than one contribution to the thermodynamic properties is present (e.g. vibrational, electronic, magnetic, etc.), the Grüneisen parameters are not additive, rather the Grüneisen parameter for the material is an average, weighted by the heat capacity contribution of each component [17]: $\gamma = \sum_r \gamma_r C_r / \sum_r C_r$.

3. Results and discussion

3.1. Thermal expansion and heat capacity

Zero field, temperature-dependent, linear ($L \| [100]$) thermal expansion coefficients for RAl$_3$ (R = Tm, Yb, Lu) (together with the literature data [18] of polycrystalline Cu for comparison), are shown in Fig. 1. In the overlapping temperature regions ($T > 90$ K), the thermal expansion coefficient values for LuAl$_3$ and YbAl$_3$ deduced from the the lattice parameters as a function of temperature data [11] are comparable to our results. At room temperature, thermal expansion values of the non-hybridizing TmAl$_3$ and LuAl$_3$ are very similar. The differences in $\alpha(T)$ between these two materials, on cooling, and in particular a peak in $\alpha(T)$ of TmAl$_3$ at ~ 20 K, are probably related

to the CEF contributions to the thermal expansion of TmAl$_3$. $\alpha(T)$ of YbAl$_3$ is lower than that of its non-magnetic analogue, LuAl$_3$, over the whole temperature range. Such behavior is consistent [20] with YbAl$_3$ being an Yb-based, intermediate valence material with a high, $T_K \gg 300$ K, Kondo temperature. Qualitatively, such behavior can be understood by noting that the fractional Yb valence in YbAl$_3$ increases with increase in temperature (in the temperature range of our measurements) [21] and that the ionic radius of Yb^{3+} is smaller than that of Yb^{2+}.

Figure 2 presents the temperature-dependent linear thermal expansion coefficient (α), the heat capacity (C_p) and the ratio α/C_p for LuAl$_3$. $\alpha_{[100]}(T)$ and $C_p(T)$ have similar temperature dependencies. The ratio of these two quantities (that, as mentioned above, is likely to approximate the temperature dependence of the Grüneisen parameter) is practically constant down to ~ 50 K, only rising at lower temperatures and manifesting a peak at ~ 8 K. It is not unusual to observe a temperature-dependent Grüneisen parameter, even in simple, non-magnetic, metals [17]. This is due to the different temperature dependencies of the electron and phonon contributions to the thermodynamic properties, with these contributions becoming comparable in magnitude at low temperatures. Additionally, the error bars in α/C_p may be somewhat enhanced at low temperatures as a result of calculating the ratio of two, diminishingly small numbers.

For TmAl$_3$ (Fig. 3) both thermal expansion and heat capacity exhibit a broad peak in the $15 - 20$ K temperature range, apparently related to CEF effects. This peak is still observable in the α/C_p curve, however, if the data are plotted as $\Delta\alpha/\Delta C_p$, (i.e. after subtraction of the non-magnetic background) it is not seen, confirming the same origin of the feature in C_p and α. The $\Delta\alpha/\Delta C_p$ shows a close to linear, slowly changing with temperature, behavior, probably representing rather well the behavior of the magnetic contribution to the Grüneisen parameter.

The peak in heat capacity evolves with applied field (Fig. 4) reflecting the lifting of the degeneracy of TmAl$_3$ energy levels. A variety of differing CEF schemes, based on fits of different experimental quantities ($C_p(T)$, or $\chi(T)$, or high field $M(H)$) were suggested for TmAl$_3$ in the literature [4, 12, 13, 14]. To analyze our magnetization, susceptibility and specific heat data we will use the approach delineated in Ref. [22]. Since Tm^{3+} ions in TmAl$_3$ have octahedron type of coordination, both parameters, W and x, of the CEF hamiltonian for cubic symmetry (see Ref. [22] for definitions of these parameters and detailed discussion) are negative and the ground state is Γ_2 (set 1) or Γ_1 (set 2). Temperature dependent susceptibility and magnetization isotherms up to 70 kOe (Fig. 5) allow for similar quality fits for CEF schemes with either ground states. Heat capacity data are better fit with the CEF scheme corresponding to Γ_2 ground state (Fig. 6) (for both sets the W and x values from fits of temperature-dependent susceptibility and magnetic isotherms were used). The W and x values for both sets are listed on the graph. An applied magnetic field changes the CEF splitting via the Zeeman term. The $H = 0$ CEF levels plus this Zeeman term describe $H = 140$ kOe

data well (Fig. 6).

Fig. 7 shows the simulation of the heat capacity behavior using the various CEF splitting schemes proposed in the literature [4, 12, 13, 14] including two of the three schemes [4] presented as indistinguishable given their low temperature data. Set 2 in Ref. [4] and the parameters from Ref. [12] are close to our results (set 1) and describe the heat capacity data reasonably well, whereas the parameters from Refs. [13, 14] and set 1 in Ref. [4] fail as reasonable approximations of the experimental data.

An applied field changes the behavior of the thermal expansion coefficient of $TmAl_3$ dramatically (Fig. 8). In between 25 kOe and 50 kOe the low temperature maximum turns into a minimum. This minimum deepens in higher fields and reaches $\approx -1.7 \cdot 10^{-5}$ K^{-1} near 15 K for $H = 140$ kOe. Clearly, as a result of the changing CEF energy scales, the Grüneisen parameter will be significantly different in the applied field. Qualitatively similar, but approximately an order of magnitude lower in size, field-induced changes in $\alpha_{[100]}(T)$ are observed in $Tm_{0.1}Lu_{0.9}Al_3$ (cf. two insets to Fig. 8). These perceptible field dependences of $\alpha_{[100]}(T)$ in both $TmAl_3$ and $Tm_{0.1}Lu_{0.9}Al_3$ are consistent with a CEF-related, single-ion effect.

To illustrate the complexity of the effect of magnetic field on the thermal expansion coefficient, data for $Er_{0.1}Lu_{0.9}Al_3$ is shown in Fig. 9. As opposed to $Tm_{0.1}Lu_{0.9}Al_3$ (Fig. 8, inset) a *positive*, broad feature in $\alpha_{[100]}(T)$ below ~ 40 K grows with increasing applied magnetic field. Transverse thermal expansion measurements in an applied field and some knowledge the CEF scheme for $Er_{0.1}Lu_{0.9}Al_3$ would be needed for comparative analysis of the effects of magnetic field on these two different materials.

For $YbAl_3$, $\alpha_{[100]}(T)$ and $C_p(T)$ (Fig. 10) have similar temperature dependencies, without any apparent striking features. The ratio of these two quantities is practically constant down to ~ 30 K and then decreases at lower temperatures. $\Delta\alpha/\Delta C_p$ is linear (and close to constant) at higher temperatures and then, on further cooling, decreases and passes through broad minimum. Given that the Kondo temperature is above room temperature [5], it is tempting to try to connect these changes in $\Delta\alpha/\Delta C_p$ to the emerging second, low temperature ($\sim 30 - 40$ K), scale in $YbAl_3$ [10], however at this point there is no clear evidence for such conjecture and more studies are required. Additionally, we cannot exclude this low temperature behavior to be the result of an interplay between phonons and (enhanced) electronic degrees of freedom. Specific heat data show an elevated electronic specific heat coefficient, $\gamma \sim 50$ mJ/mol K^2, for $YbAl_3$, significantly higher than that for $LuAl_3$, in consistence with the intermediate valence nature of $YbAl_3$ and similar to recently reported data [23].

$\alpha_{[100]}(T)$ for $YbAl_3$ is not significantly affected by an applied magnetic field of 140 kOe (Fig. 11). This is not surprising for a material with a high, $600 - 700$ K, Kondo temperature. At low temperatures ($T \leq 20$ K) $YbAl_3$ exhibits a region of negative thermal expansion, $\alpha_{[100]}(T) < 0$. For $Yb_{0.1}Lu_{0.9}Al_3$ the region of negative thermal expansion does not appear (above 1.8 K) since $\alpha_{[100]}(T)$ is apparently dominated by the

contribution from the LuAl$_3$ matrix. Both, in pure YbAl$_3$ and diluted Yb$_{0.1}$Lu$_{0.9}$Al$_3$, the temperature dependent thermal expansion is below the one for the non-magnetic analogue, LuAl$_3$, consistent with an intermediate valence character of the Yb ion in pure and diluted material.

3.2. Magnetostriction and quantum oscillations

In LuAl$_3$ the base temperature (1.8 K) magnetostriction is rather small, however, starting at fields below 40 kOe de Haas-van Alphen (dHvA) like oscillations in magnetostriction (Fig. 12) are clearly observed. A fast Fourier transform performed on these data in the form of $\Delta L/L_0$ vs. $1/H$. Seven dHvA frequencies ranging from ~ 1 MG to ~ 50 MG were observed (Fig. 12, inset). The occurrence of quantum oscillations in magnetostriction is a known phenomenon [24], however observations of such oscillations are rather rare, since both large, high quality single crystals and sensitive dilatometers are required. dHvA oscillations were observed in LuAl$_3$ via magnetostriction up to temperatures as high as 20 K (Fig. 13). The temperature dependence of the amplitude of these oscillations can be used to evaluate the effective masses of the quasiparticles on the corresponding extremal orbits using standard Lifshitz - Kosevich formula [25, 26, 27]. The obtained dHvA frequencies and corresponding effective masses, m^*/m_0, together with the literature data [28] obtained by a conventional magnetic susceptibility field-modulation technique are shown in Fig. 14. Of the seven orbits observed in this work, four (above 10 MG) are consistent with experimental or theoretical literature data and three frequencies ($F < 10$ MG, $m^*/m_0 < 0.5$) are new.

The magnetostriction of YbAl$_3$ is also rather small: $\Delta L/L_0 \approx 3 \cdot 10^{-9}$ at $T = 1.8$ K, $H = 140$ kOe. In high fields dHvA-like oscillations are also observed (Fig. 15). The amplitude of the oscillations is significantly smaller (few orders of magnitude for the leading frequency) than that for LuAl$_3$ and they reduce to the level of noise above ~ 15 K. Two frequencies and their effective masses were identified from our measurements and the results are plotted together with the literature data in Fig. 16. It is worth noting that, for the orbits detected by magnetostriction the electronic masses in YbAl$_3$ are similar to those found for LuAl$_3$. Significant mass enhancement appears to occur only for higher frequencies.

Longitudinal magnetostriction of TmAl$_3$ is orders of magnitude higher than that of YbAl$_3$ and LuAl$_3$: $\Delta L/L_0 \approx 7 \cdot 10^{-4}$ at $T = 1.8$ K, $H = 140$ kOe (Fig. 17). In the intermediate and high fields the magnetostriction is approximately proportional to H^2 (Fig. 17, inset). Detailed analysis of the magnetostriction [31, 32, 33] requires knowledge of the details of the Tm3$^+$ ion-lattice interactions.

We can not resolve quantum oscillations of magnetostriction in TmAl$_3$, although there are no indications of inferior crystal quality. We need to mention though that the much higher, monotonic magnetostriction background makes observation of quantum

oscillations extremely difficult. Using a traditional magnetic susceptibility modulation technique seven fundamental dHvA frequencies were observed in TmAl$_3$ for $H\|[100]$ [34], these frequencies being similar to the ones found for LuAl$_3$ and YbAl$_3$.

4. Summary

Temperature-dependent thermal expansion coefficients were measured between 1.87 K and 300 K for RAl$_3$ (R = Lu, Yb, Tm) along [100] direction. In YbAl$_3$ the intermediate valence of the Yb-ions results in $\alpha(T)$ for this material being consistently lower than $\alpha(T)$ of the non-magnetic analogue, LuAl$_3$, with a negative thermal expansion region at low temperatures. Thermal expansion coefficient, $\alpha(T)$, of TmAl$_3$ manifests contribution from the CEF effects and, as opposed to YbAl$_3$ and LuAl$_3$, displays strong field dependence below ~ 100 K.

Magnetostriction of YbAl$_3$ and LuAl$_3$ ($H\|L\|[100]$) shows clear dHvA-like oscillations up to temperatures as high as above 20 K for LuAl$_3$. Several new dHvA frequencies were measured (three for LuAl$_3$ and two for YbAl$_3$) and their effective masses were estimated. For these orbits the electronic masses in YbAl$_3$ are similar to those found for LuAl$_3$. TmAl$_3$ shows very large, exceeding that of YbAl$_3$ and LuAl$_3$ by several orders of magnitude, magnetostriction at low temperatures.

In addition, a CEF splitting scheme for TmAl$_3$ with the Γ_2 level as the ground state is strongly suggested based on the analysis of the heat capacity to significantly higher fields and temperatures. This result removes a two decade ambiguity as to the CEF level scheme for this material.

Acknowledgments

References

[1] van Vucht J H N, Buschow K H J 1965 *J. Less-Common Metals* **10** 98.
[2] Bargouth M O, Will G 1971 *Phys. Lett. A* **36** 50.
[3] Buschow K H J 1965 *Zeit. Physik. Chem.* **59** 21.
[4] Deutz A F, Brom H B, Huiskamp W J, de Jongh L J, Buschow K H J 1989 *Physica B* **160** 83.
[5] Havinga E E, Buschow K H J, van Daal H J 1973 *Solid State Comm.* **13** 621.
[6] Hiess A, Boucherle J X, Givord F, Schweizer J, Lelievre-Berna E, Tasset F, Gillon B, Canfield P C 2000 *J. Phys.: Cond. Mat.* **12** 829.
[7] Ebihara T, Bauer E D, Cornelius A L, Lawrence J M, Harrison N, Thompson J D, Sarrao J L, Hundley M F, Uji S 2003 *Phys. Rev. Lett.* **90** 166404.
[8] Bauer E D, Booth C H, Lawrence J M, Hundley M F, Sarrao J L, Thompson J D, Riseborough P S, Ebihara T 2004 *Phys. Rev. B* **69** 125102.

[9] Christianson A D, Fanelli V R, Lawrence J M, Goremychkin E A, Osborn R, Bauer E D, Sarrao J L, Thompson J D, Frost C D, Zarestky J L 2006 *Phys. Rev. Lett.* **96** 117206.

[10] Cornelius A L, Lawrence J M, Ebihara T, Risenborough P S, Booth C H, Hundley M F, Pagliuso P G, Sarrao J L, Thompson J D, Jung M H, Lacerda A H, Kwei G H 2002 *Phys. Rev. Lett.* **88** 117201 .

[11] Iandelli A, Palenzona A 1972 *J. Less-Common Metals* **29** 293.

[12] Bucher E, Maita J P, Hull Jr. G W, Sierro J, Chu C W, Luthi B 1974 *Proc. 1-st Conf. on Cryst. Elec. Field Effects in Metals and Alloys* (Montreal) edited by Devine R A V, 221.

[13] de Wijn H W, van Diepen A M, Buschow K H J 1970 *Phys. Rev. B* **1** 4203.

[14] Sugiyama K, Futoh M, Iizuka T, Ebihara T, Inoue T, Kindo K, Ōnuki Y 2001 *J. Phys. Soc. Jpn.* **70** 3753.

[15] Canfield P C, Fisk Z 1992 *Philos. Mag. B* **65** 1117 .

[16] Schmiedeshoff G M, Lounsbury A W, Luna D J, Tracy S J, Schramm A J, Tozer S W, Correa V F, Hannahs S T, Murphy T P, Palm E C, Lacerda A H, Bud'ko S L, Canfield P C, Smith J L, Lashley J C, Cooley J C 2006 *Rev. Sci. Instrum.* **77** 123907.

[17] Barron T H K, White G K 1999 *Heat Capacity and Thermal Expansion at Low Temperatures* (New York, NY: Kluwer Academic/Plenum Publishers)

[18] Kroeger F R, Swenson C A 1977 *J. Appl. Phys.* **48** 853.

[19] Pott R, Schefzyk R, Wohlleben D, Junod A 1981 *Z. Phys. B* **44** 17.

[20] Wohlleben D K in: Falicov L M, Hanke W, Maple M B (editors) 1981 *Valence Fluctuations in Solids* (Amsterdam: North-Holland), p. 1

[21] Sales B C, Wohlleben D K 1975 *Phys. Rev. Lett.* **35** 1240.

[22] Lea K R, Leask M J M, Wolf W P 1962 *J. Phys. Chem. Solids* **23** 1381.

[23] Urbano R R, Bittar E M, Pires M A, Mendonça Ferreira A L, Bufaiçal L, Rettori C, Pagliuso P G, Magill B, Oseroff S B, Thompson J D, Sarrao J L 2007 *Phys. Rev. B* **75** 045107.

[24] Chandrasekhar B S, Fawcett E 1971 *Adv. Phys.* **20** 775.

[25] Lifshitz I M, Kosevich A M 1954 *Dokl. Akad. Nauk SSSR* **96** 963.

[26] Lifshitz I M, Kosevich A M 1955 *Zh. Exper. Teor. Fiz.* **29** 730 (translation: 1956 *Sov. Phys. JETP* **2** 636).

[27] Shoenberg D 1984 *Magnetic Oscillations in metals* (Cambrigde: Cambridge University Press).

[28] Sakamoto I, Chen G F, Ohara S, Harima H, Maruno S 2001 *J. Alloys Comp.* **323-324** 623.

[29] Ebihara T, Uji S, Terakura C, Terashima T, Yamamoto E, Haga Y, Inada Y, Onuki Y 2000 *Physica B* **281-282** 754.

[30] Ebihara T, Inada Y, Murakawa M, Uji S, Terakura C, Terashima T, Yamamoto E, Haga Y, Ōnuki Y, Harima H 2000 *J. Phys. Soc. Jpn.* **69** 895.

[31] Nicholson K, Häfner U, Müller-Hartmann E, Wohlleben D 1978 *Phys. Rev. Lett.* **41** 1325.

[32] Campbell I A, Creuset G, Sanchez J 1979 *Phys. Rev. Lett.* **43** 234.

[33] Creuset G, Campbell I A 1981 *Phys. Rev. B* **23** 3375.

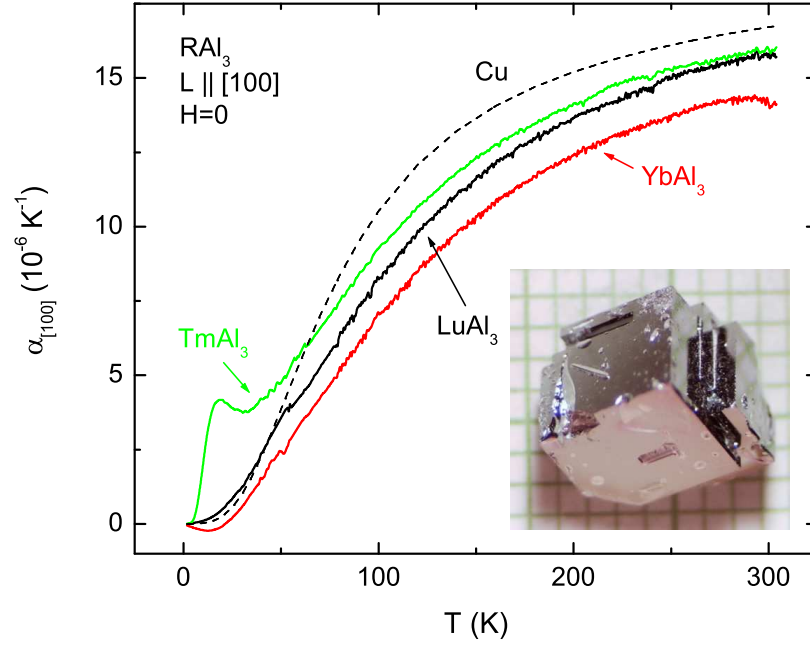[34] Ebihara T, Aoki D, Inada Y, Settai R, Sugiyama K, Haga Y, Onuki Y 2001 *J. Magn. Magn. Mat.* **226-230** 101.

Figure 1. (Color online) Temperature-dependent linear thermal expansion coefficients along [100] direction of RAl$_3$ (R = Tm, Yb, Lu) in zero applied field. Data for polycrystalline Cu [18] are shown as dashed line for comparison. Inset: LuAl$_3$ crystal over a mm scale.
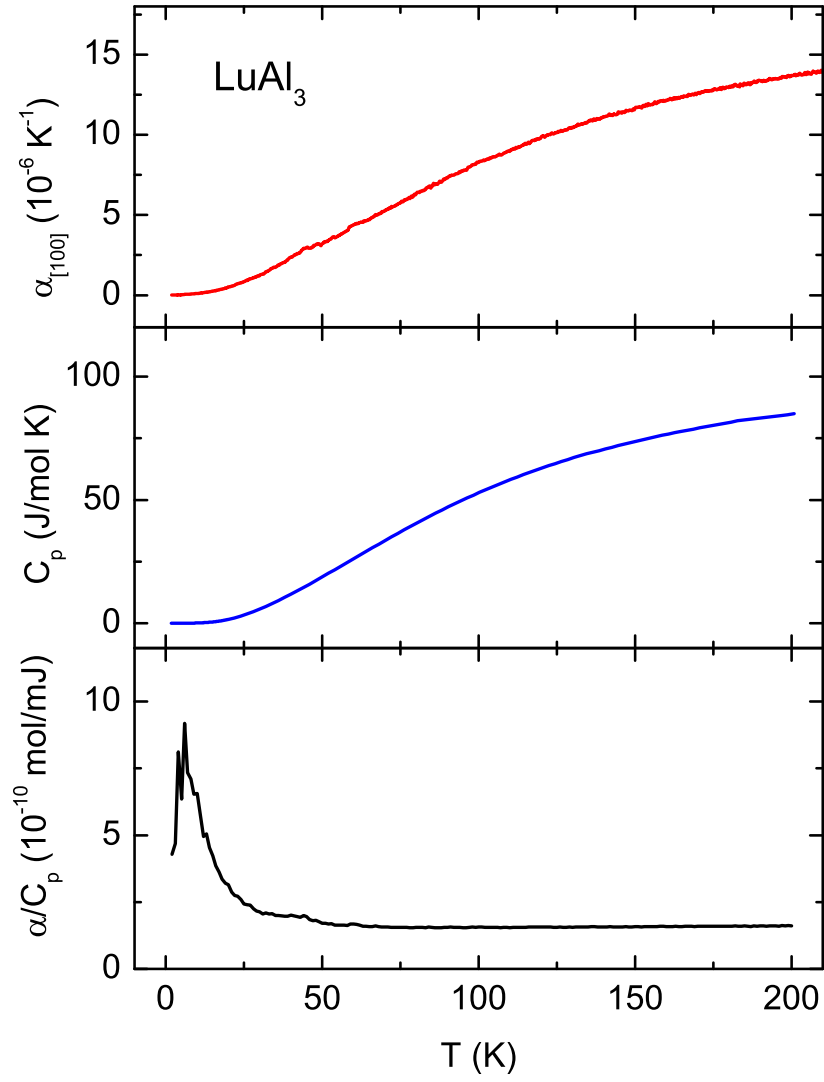
Figure 2. (Color online) Temperature-dependent linear thermal expansion coefficient, heat capacity and the ratio α/C_p for LuAl$_3$ in zero applied field.
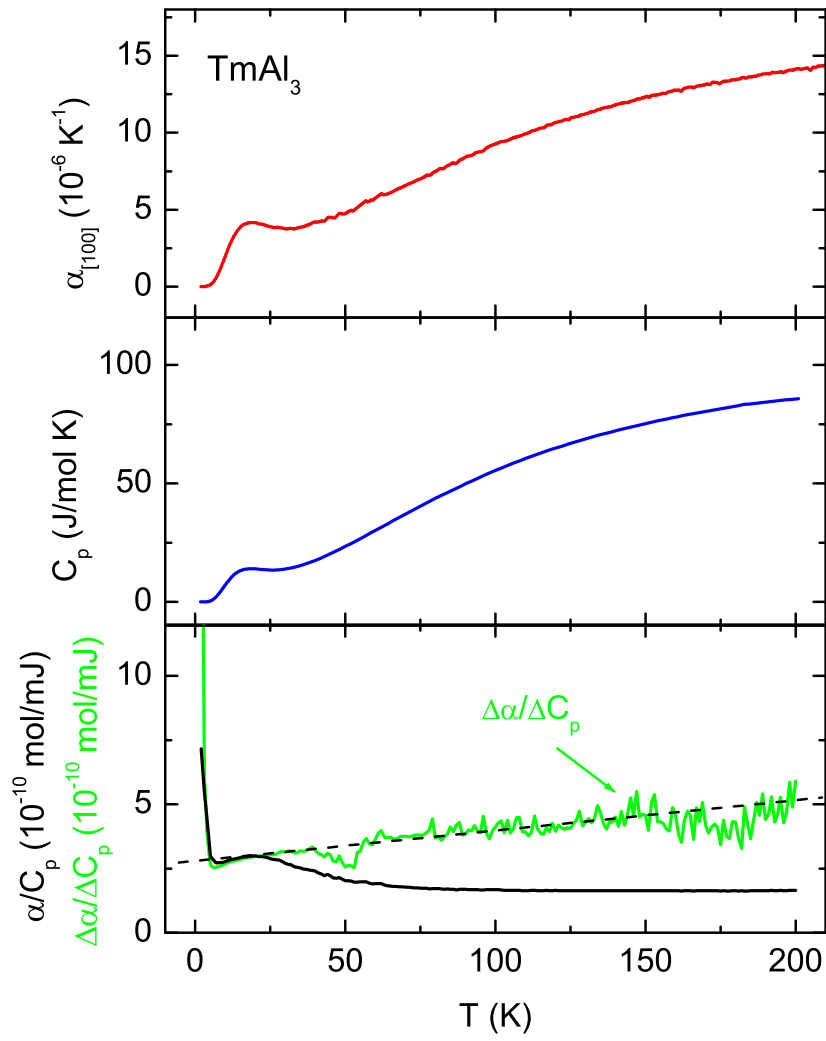
Figure 3. (Color online) Temperature-dependent linear thermal expansion coefficient, heat capacity and the ratio α/C_p for TmAl$_3$ in zero applied field. Additionally, on the lower panel $\Delta\alpha/\Delta C_p = (\alpha(\text{TmAl}_3) - \alpha(\text{LuAl}_3))/(C_p(\text{TmAl}_3) - C_p(\text{LuAl}_3))$ is plotted. Dashed line is a guide for the eye.
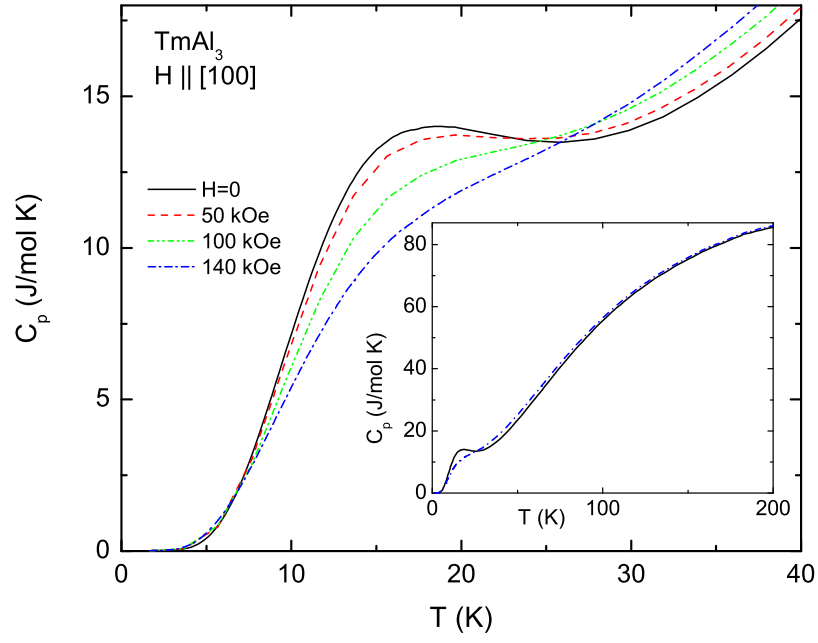
Figure 4. (Color online) The low temperature part of heat capacity for TmAl₃ in applied fields $H = 0, 50, 100, 140$ kOe. Field was applied along [100] axis. Inset: data for $H = 0$ and 140 kOe up to 200 K.
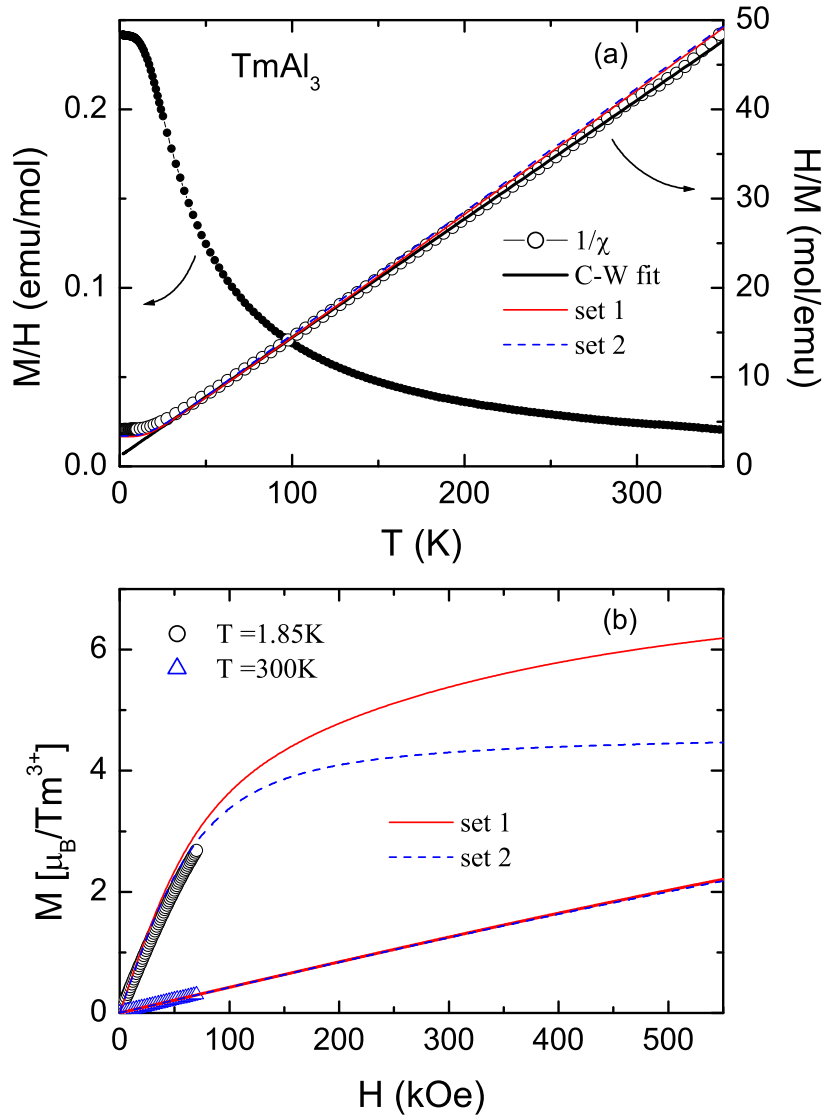
Figure 5. (Color online) (a) Temperature-dependent magnetic susceptibility, M/H, inverse magnetic susceptibility, H/M, taken at $H = 1$ kOe, $H\|[100]$ and (b) magnetization isotherms, $M(H)$, for $T = 1.85$ K and 300 K for TmAl$_3$. Curie - Weiss fit of inverse magnetic susceptibility and CEF simulations of H/M and $M(H)$ for two possible sets of parameters (set 1: $W = -1.011, x = -0.298$ set 2: $W = -2.125, x = -0.682$) are show as lines.
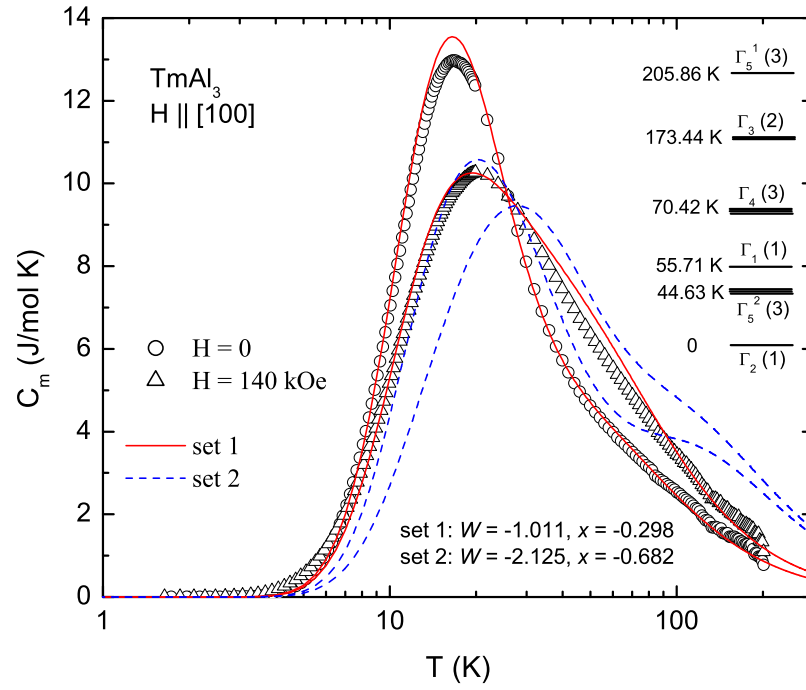
Figure 6. (Color online) Magnetic contribution to the heat capacity of TmAl₃, $C_m = C_p^{TmAl_3} - C_p^{LuAl_3}$, in zero and 140 kOe ($H\|[100]$) applied field. CEF simulations for two possible sets of parameters are show as lines. Corresponding W and x values are listed for both sets are listed. CEF scheme for set 1 is illustrated in the right side of the plot.
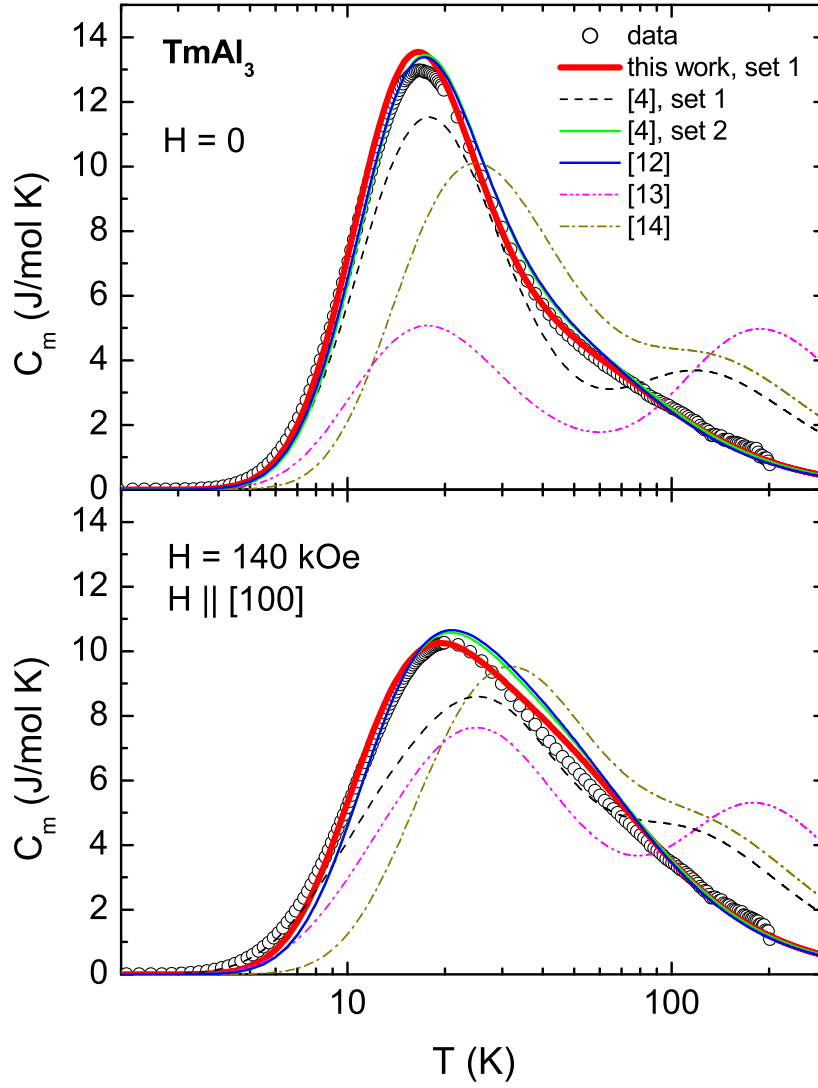
Figure 7. (Color online) Magnetic contribution to the heat capacity of TmAl$_3$, $C_m = C_p^{TmAl_3} - C_p^{LuAl_3}$, in zero and 140 kOe ($H \parallel [100]$) applied field. CEF simulations using set 1 from this work and the literature data are show as lines. The following W and x values (listed as $\{W, x\}$) were used: this work, set 1: $\{-1.011, -0.298\}$; Ref. [4], set 1: $\{1.95, 0.82\}$, set 2: $\{-0.993, -0.282\}$; Ref. [12]: $\{-0.94, -0.27\}$; Ref [13]: $\{3.24, -0.8\}$; Ref [14]: $\{-2.316, -0.827\}$
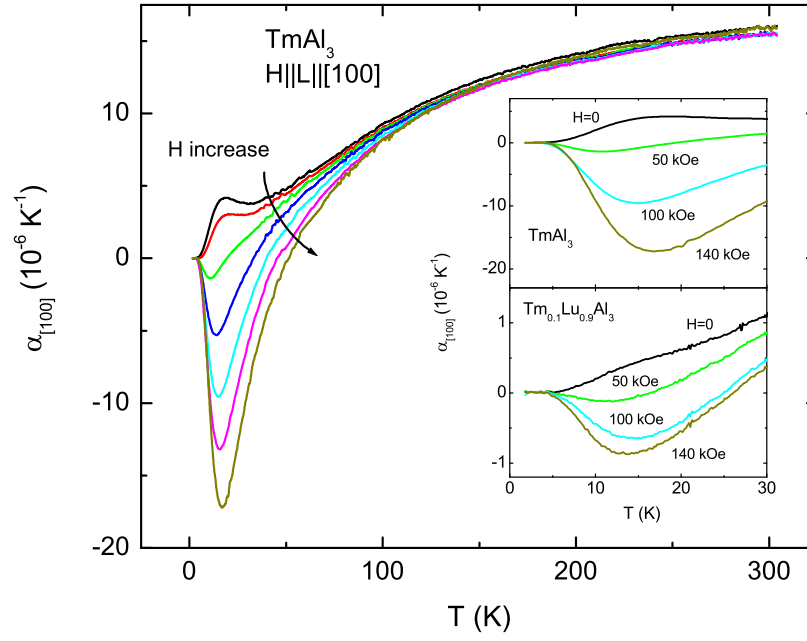
Figure 8. (Color online) Temperature-dependent linear thermal expansion coefficient for TmAl$_3$ in applied fields of $0, 25, 50, 75, 100, 125, 140$ kOe. Insets: low temperature part of $\alpha(T)$ in $0, 50, 100, 140$ kOe applied fields for TmAl$_3$ and Tm$_{0.1}$Lu$_{0.9}$Al$_3$.
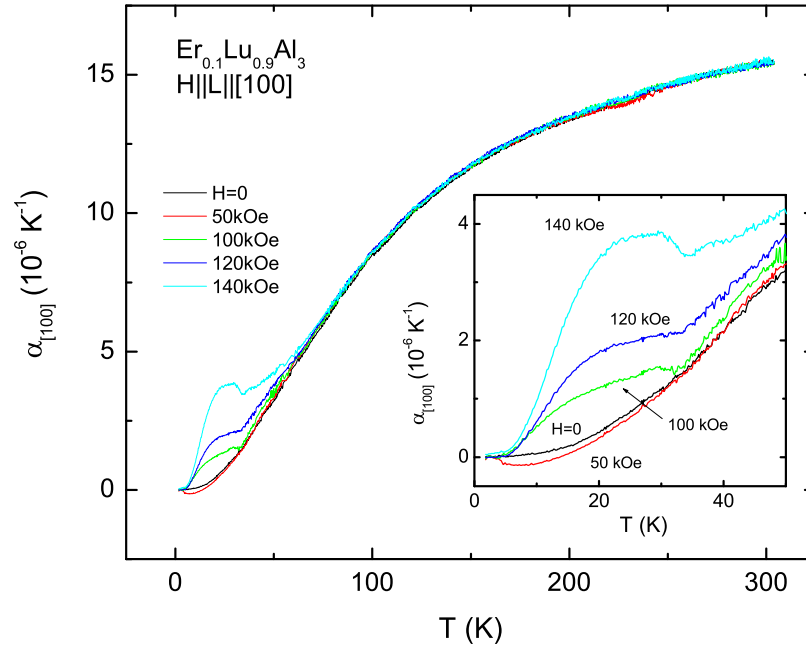
Figure 9. (Color online) Temperature-dependent linear thermal expansion coefficient for Er$_{0.1}$Lu$_{0.9}$Al$_3$ in applied fields of $0, 50, 100, 120, 140$ kOe. Insets: low temperature part of $\alpha(T)$.
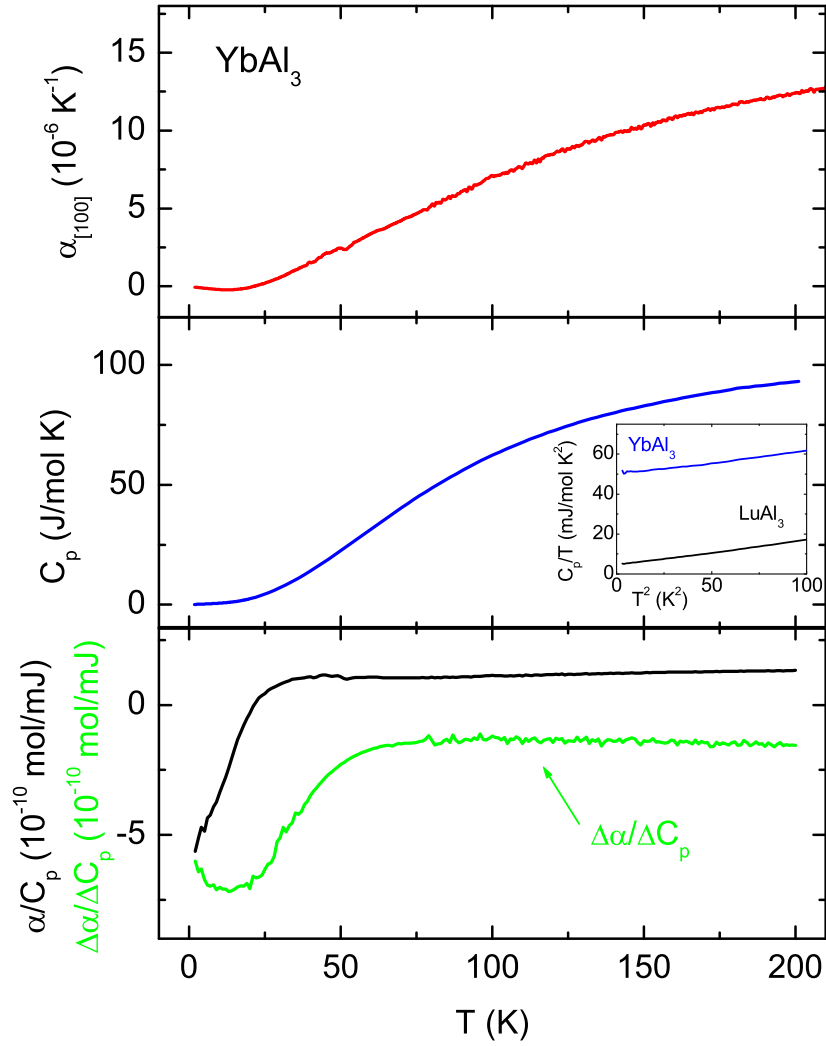
Figure 10. (Color online) Temperature-dependent linear thermal expansion coefficient, heat capacity and the ratio α/C_p for YbAl$_3$ in zero applied field. Additionally, on the lower panel $\Delta\alpha/\Delta C_p = (\alpha(\text{YbAl}_3) - \alpha(\text{LuAl}_3))/(C_p(\text{YbAl}_3) - C_p(\text{LuAl}_3))$ is plotted. Inset: low temperature C_p/T vs. T^2 for LuAl$_3$ and YbAl$_3$.
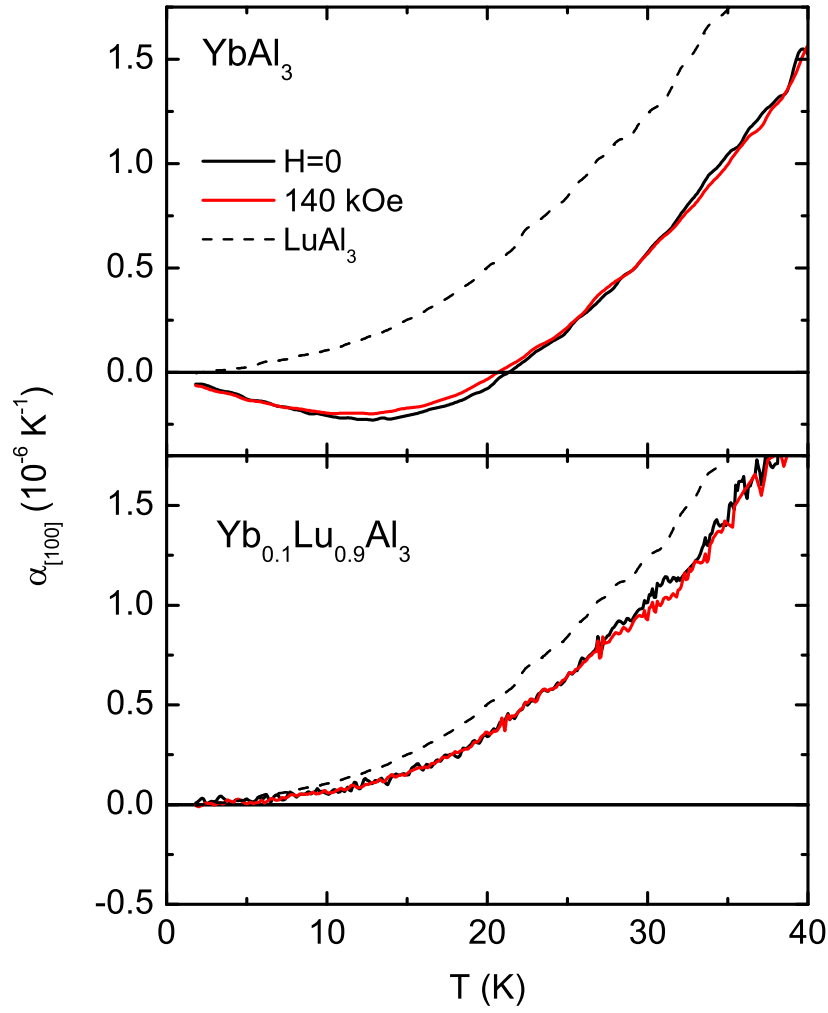
Figure 11. (Color online) Low temperature part of linear thermal expansion coefficient for YbAl$_3$ and Yb$_{0.1}$Lu$_{0.9}$Al$_3$ in applied fields of 0 and 140 kOe. For comparison, data for LuAl$_3$ are shown as dashed line.
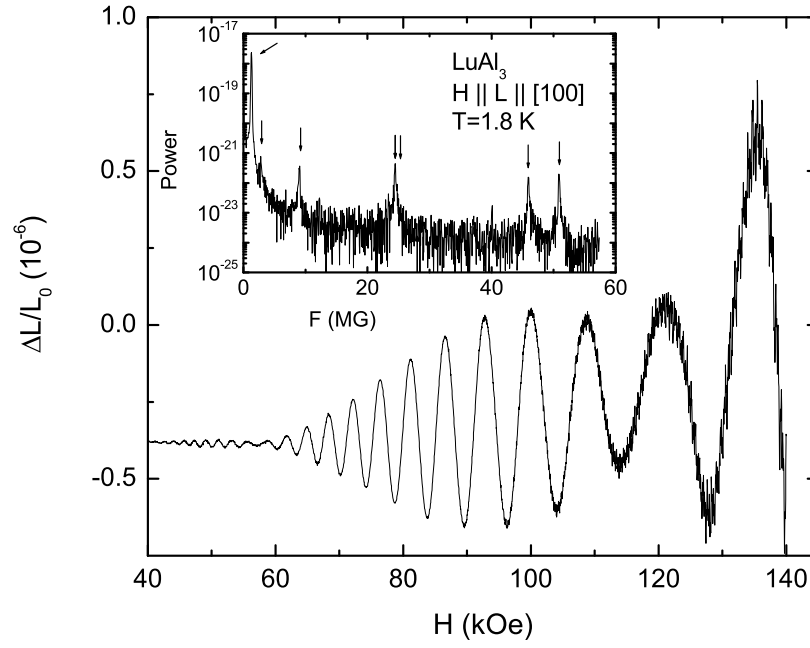
Figure 12. High field part of longitudinal ($H\|L\|[100]$) magnetostriction in LuAl₃ measured at 1.8 K. Inset: fast Fourier transform of the corresponding $\Delta L/L_0$ vs. $1/H$ data. Arrows mark the de Haas-van Alphen frequencies.
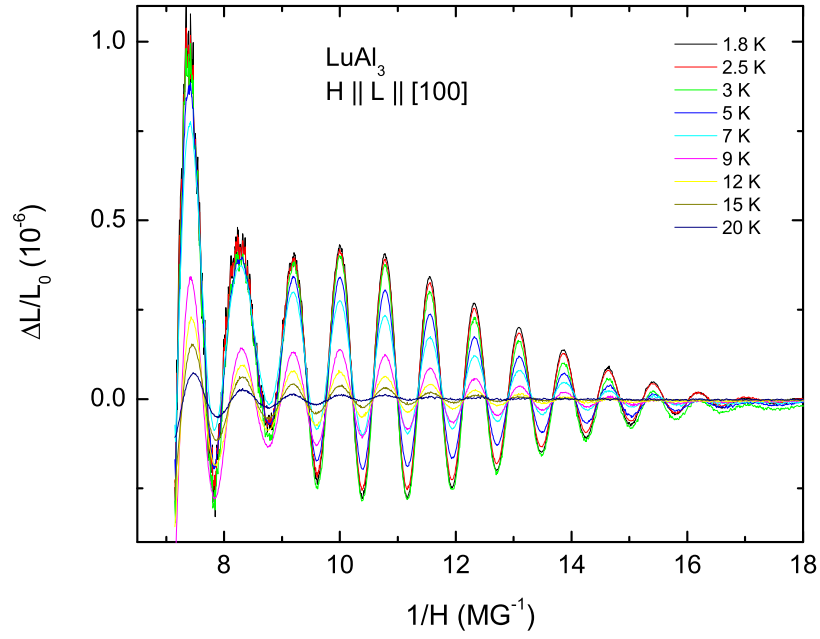
Figure 13. (Color online) Longitudinal magnetostriction in LuAl$_3$ for $H\|[100]$ at different temperatures, from 1.8 K to 20 K plotted as a function of $1/H$. Constant background was subtracted from the data.
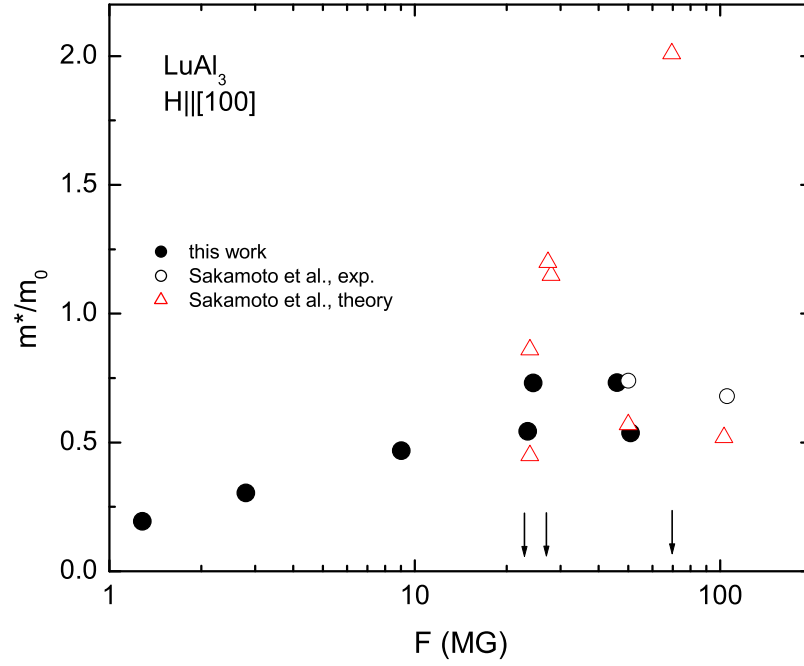
Figure 14. (Color online) dHvA frequencies and corresponding effective masses for LuAl₃, $H\|[100]$. Filled circles - this work, other symbols - literature data [28]: open circles - experiment, triangles - theory. Note that Sakamoto et al. experimentally identified several other dHvA frequencies but did not determine the corresponding effective masses. These experimental frequencies are shown by arrows.
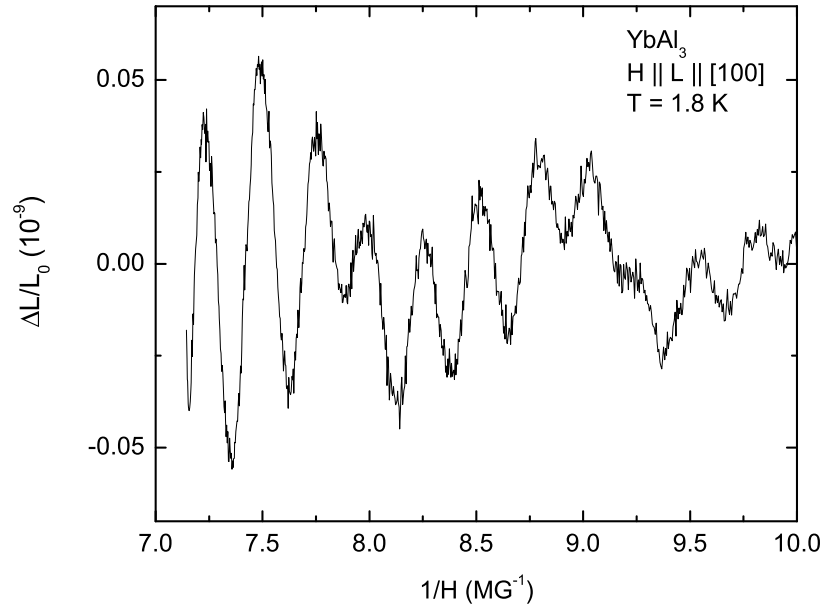
Figure 15. Longitudinal magnetostriction in YbAl$_3$ for $H\|[100]$ at $T = 1.8$ K plotted as a function of $1/H$. Constant background was subtracted from the data.
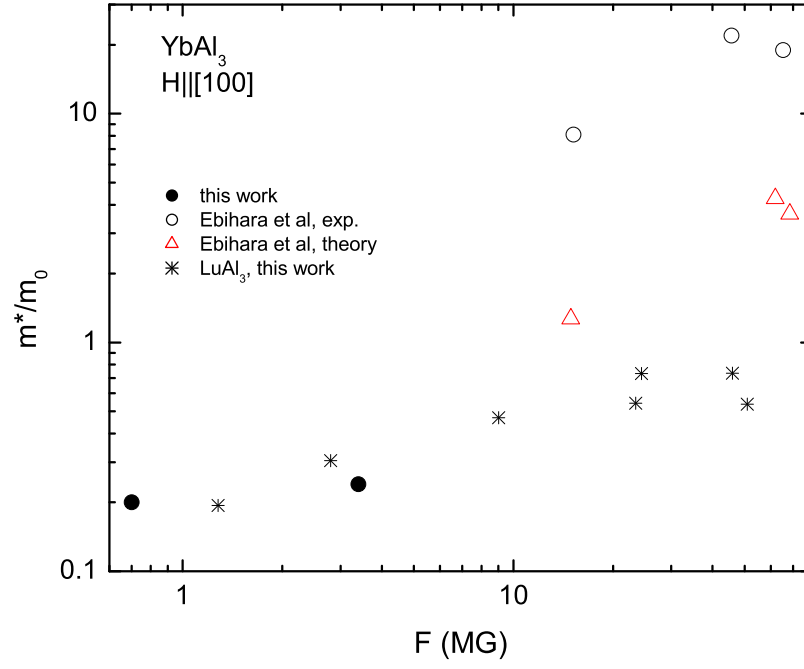
Figure 16. (Color online) dHvA frequencies and corresponding effective masses for YbAl₃, $H\|[100]$. Filled circles - this work, other symbols - literature data: open circles - experiment [29], triangles - theory [30]. Data for LuAl₃ (this work) are shown as asterisks for comparison.
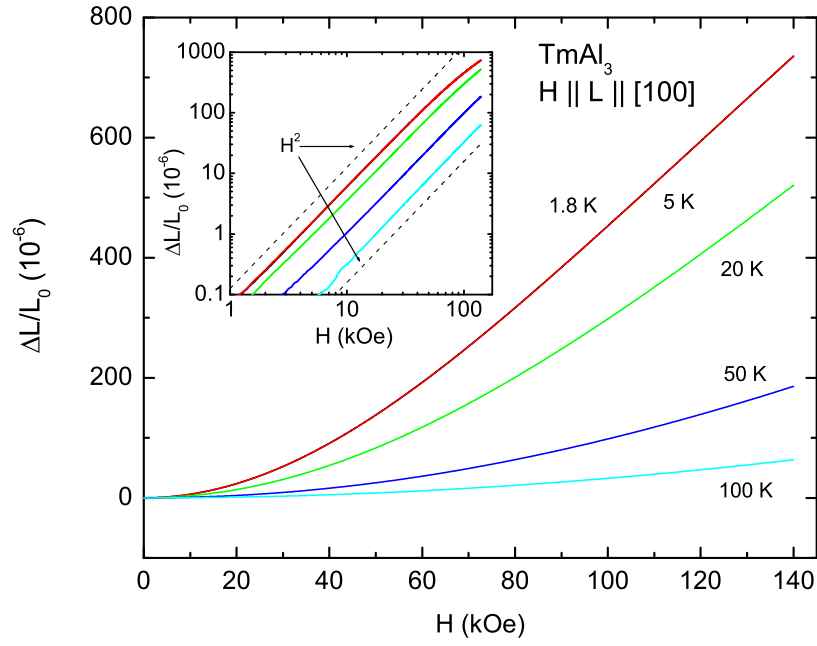
Figure 17. (Color online) Longitudinal magnetostriction in TmAl$_3$ for $H\|[100]$ at different temperatures, from 1.8 K to 100 K. Note that within the scale of the plot, 1.8 K and 5 K data coincide. Inset: the same data on a *log - log* plot. Dashed lines correspond to $\Delta L/L_0 \propto H^2$ functional behavior.